RSC Advances

PAPER

View Article Online
View Journal | View Issue

Cite this: *RSC Adv.*, 2014, **4**, 30375

Understanding the photothermal effect of gold nanostars and nanorods for biomedical applications

Xiaocui Wang,[ab] Guohua Li,[ab] Yu Ding[ab] and Shuqing Sun*[a]

Received 3rd April 2014
Accepted 17th June 2014

DOI: 10.1039/c4ra02978j

www.rsc.org/advances

The plasmon-based photothermal effect of gold nanorod (GNR) has undergone the most systematic investigation for cancer therapy in the biomedical realm. In recent years, gold nanostar (GNS) has come into sight with its attractive ability to transduce electromagnetic radiation into heat. Understanding photothermal conversion efficiency is thus becoming more important for the selection of suitable materials for photothermal therapy. In this article, we investigated systematically the photothermal conversion efficiency and the molar heating rate of GNS and GNR in three groups (S-group, M-group and L-group, representing groups of nanostructures with central extinctions at shorter, medium and longer wavelengths, respectively), to better understand the behaviour of GNS and GNR in the field of photothermal therapy. In the M-group and L-group, the photothermal conversion efficiencies of GNSs and GNRs are similar, while GNSs have a much higher molar heating rate than GNRs. Among all the samples, L-GNS has the highest molar heating rate, because of its large molar extinction coefficient. In addition, the discrete dipole approximation (DDA) was employed to simulate the optical properties of gold nanoparticles with different shapes, and the photothermal properties of GNSs and GNRs were compared experimentally and theoretically. From both the experimental and the theoretical results, M-GNS and L-GNS exhibit higher extinction efficiencies than M-GNR and L-GNR, respectively.

1. Introduction

Hyperthermia has been used to destruct tumours for decades, and various heat sources, including microwaves,[1,2] ultrasound[3] and laser light,[4,5] have been employed to investigate thermal therapy. Laser-induced photothermal therapy for cancer treatment has been widely investigated, due to its ability to deliver a specific amount of energy directly to cancerous tissue.[6–8] Near-infrared (NIR) light is an ideal electromagnetic source for the application of photothermal therapy, because it can transmit deeply in biological tissues.[9] Various kinds of nanomaterials have been employed in photothermal therapy, including hydrophilic flower-like CuS superstructures,[10] single-walled carbon nanotubes (SWNTs),[11,12] graphene oxide,[13] gold nanospheres,[14] gold nanocages,[15,16] gold nanoshells,[17,18] gold nanopyramids,[19] gold nanorods (GNRs),[20,21] and gold nanostars (GNSs).[22] These nanostructures have the ability to convert NIR light into heat on a picosecond timescale, which causes an increase in the temperature of the surrounding environment, and can lead to the damage of tumour cells.[23,24]

GNR is an ideal nanocrystal for the photothermal treatment of cancer and tumours. In recent years, GNRs have been extensively researched and to some extent have become a standard for the evaluation of the photothermal effects of other nanostructures. It has been found that the photothermal conversion efficiency of nanocrystals is strongly affected by several factors, including plasmon resonance, shell coating, nanocrystal volume and assembly state.[25] To improve the photothermal efficiency and the heating speed of GNRs, a supercontinuum light can be used as a fast, energy-efficient excitation source, delivered in femtosecond pulses.[26] In addition, biodegradable plasmonic vesicles, consisting of GNRs carrying mixed polymer brushes, contribute to optimizing the photothermal conversion property of GNRs.[27] Because of their attractive photothermal conversion efficiency, GNRs have been used *in vitro* and *in vivo*, and have shown outstanding curative effects. GNRs covalently linked with primary antibodies specific to the Gram-negative bacterium can destroy *Pseudomonas aeruginosa* cells with high efficiency.[28] It is notable that the surface chemistry of GNRs has a dominant role in the process of cellular uptake, and negatively charged GNRs can have a significant photothermal therapeutic benefit.[29,30] Recently, a dual-function nano-system of photodynamic therapy (PDT) and photothermal therapy (PTT) has been remarkably synergistic in cancer cell treatment.[31,32]

In recent years, GNS, a new type of gold nanostructure, has demonstrated potential application in biomedical areas, due to

[a]*Shenzhen Key Laboratory for Minimal Invasive Medical Technologies, Graduate School at Shenzhen, Tsinghua University, Shenzhen 518055, China. E-mail: sun.shuqing@sz.tsinghua.edu.cn*

[b]*Department of Physics, Tsinghua University, Beijing 100084, China*

several outstanding properties. GNSs have multiple sharp tips, which act as 'hot spots' due to the 'lightning rod' effect.[33] They have therefore been extensively used as substrates in surface enhanced Raman scattering spectroscopy (SERS).[34,35] In addition to the 'lightning rod' effect, GNSs have tunable plasmon bands and strong absorption in NIR regions,[36] which make them an attractive nanoplatform in various biomedical fields, including PTT,[37] PDT[38] and photoacoustic imaging.[39] Numerical calculations of the localized surface plasmon resonances of GNSs have been performed using the finite-difference time-domain (FDTD) method[40] and the 3D Green's Theorem method.[41] As GNSs have a large absorption cross section in the near infrared wavelength region, they show great potential in the field of photothermal therapy.[42] GNSs conjugated with specific nanobodies can cause cell damage at certain laser power densities.[37] Moreover, GNSs linked with a functionalized photosensitizer can be employed in a dual system of PDT and PTT to improve the anticancer effect and simplify the therapeutic process.[43] The photothermal conversion efficiency of GNSs can be greatly enhanced by coating them with polypyrrole, and the polypyrrole shell contributes significantly to the structural stability of the GNSs.[44]

In this article, the photothermal properties of three groups GNSs and GNRs with different plasmon resonance wavelengths (683 nm, 774 nm, and 821 nm) were measured and simulated. From the photothermal measurements, the photothermal conversion efficiencies of GNSs and GNRs were calculated and compared. The molar heating rate, closely related to the photothermal conversion efficiency and the molar extinction coefficient, was also calculated. This parameter is more meaningful in practice for photothermal applications. In addition, three optical parameters, including extinction efficiencies and absorption efficiencies, were calculated and compared with simulations using the discrete dipole approximation (DDA). The results demonstrate that GNSs, with their large extinction coefficient, are an excellent candidate for the photothermal treatment of cancer and tumours, despite their large scattering cross section.

2. Experiment section

2.1 Chemicals

Gold(III) chloride trihydrate ($HAuCl_4 \cdot 3H_2O$) was supplied by Sigma-Aldrich. Polyvinylpyrrolidone (PVP, MW = 8000), cetyltrimethylammonium bromide (CTAB), sodium borohydride ($NaBH_4$) and L-ascorbic acid (AA) were purchased from Alfa Aesar. *N*,*N*-dimethylformamide (DMF), hydrochloride (HCl, 37%), silver nitrate ($AgNO_3$) and sodium citrate were purchased from local chemical companies. All the chemicals were used as received without further purification. Ethanol and deionized water (18 MΩ) were used for all experiments.

2.2 Preparation of GNSs and GNRs

We used seed-mediated growth for the synthesis of both GNSs[36,45] and GNRs.[46–48] Gold nanoparticles with smaller size were first synthesized as seeds, and gold nanostructures of different shape were then formed with the help of various surfactants.

2.2.1 Synthesis of GNSs. Water-soluble gold nanoparticles of 16 nm size were prepared using the classical approach of standard citrate reduction. 50 mg of sodium citrate was dissolved in 50 mL of water, and 12.5 mL $HAuCl_4$ (1 mg mL^{-1}) was diluted to 100 mL with deionized water. Both solutions were heated in a water bath at 60 °C for about 30 minutes. Then the sodium citrate solution was added rapidly to the solution of $HAuCl_4$ with continuous stirring, the temperature of the water bath was increased to 85 °C and the mixed solution was heated for 2.5 h. The solution changed from light yellow to purple and finally presented as clear wine red. After the gold colloid was cooled to room temperature, 1.2 mL of an aqueous solution of 0.1 g mL^{-1} PVP was added, and allowed to react over 24 h. The aqueous solution provided at least 60 molecules of PVP per square nanometre of gold nanoparticles, which protected the gold nanoparticles from aggregating. Finally, the solution of gold nanoparticles capped by PVP was centrifuged at 10 000 rpm for 30 min, the supernatant was discarded and the gold nanoparticles were redispersed in 2 mL of ethanol. For the growth of GNSs, 217 μL of 25.8 mM $HAuCl_4$ was mixed with 20 mL of 10 mM PVP solution in DMF. A particular volume of preformed seed dispersion was added rapidly to the PVP solution under continuous stirring and allowed to react at room temperature until completion of the reaction (no further change in the colour of the mixture). In the experiment, we could get GNS with different sizes by varying the volume of seed dispersion. The GNS colloid was centrifuged at 10 000 rpm for 10 min, the supernatant was removed and the branched nanoparticles were resuspended in deionized water for morphology and photothermal experiments.

2.2.2 Synthesis of GNRs. For the preparation of GNRs, 3–5 nm gold nanoparticles were first synthesized. 38.1 μL of 25.8 mM $HAuCl_4$ solution was mixed with 4 mL 100 mM CTAB solution. Then, 24 μL of 100 mM ice-cold $NaBH_4$ solution was added to the mixture all at once under vigorous stirring for 2 min, which resulted in the formation of a tea-brown seed solution. After the seed solution was stirred, it was kept at 25 °C for at least 2 h, for future use. For the growth of GNRs, 943 μL of 25.8 mM $HAuCl_4$ solution was added to 50 mL 200 mM CTAB solution at 25 °C, and the mixture appeared bright yellow in colour. To this mixture, 375 μL of 5 M HCl solution, 120 μL of 40 mM $AgNO_3$ solution and 400 μL of 100 mM freshly prepared AA solution were added in sequence. Because of the mild reduction of AA, the growth solution changed from bright yellow to colourless. Finally, 70 μL of the seed solution was quickly injected into the growth solution and stirred for 30 seconds. The growth solution was left undisturbed in a 30 °C thermostat overnight. GNRs with different aspect ratios were obtained by changing the amount of $AgNO_3$. The GNRs so obtained were purified by centrifugation at 7000 rpm for 10 min to remove excess surfactant, and were redispersed in deionized water for future use.

2.3 Instrumentation

We used a UV-visible spectrophotometer (DU 800) to measure the extinction spectroscopy of the gold nanostructures. Raw spectra were integrated from 400 to 1100 nm, with a wavelength

step of 0.5 nm. Transmission electron microscopy (TEM) was performed to record the morphology of the gold nanostructures using a Tecnai G^2 30 instrument (120 kV). To prepare samples for TEM, 8 μL of the gold colloid was deposited onto a copper grid and left to dry in air. Images were captured from different regions of each copper grid to determine the distribution of gold nanostructures.

2.4 Measurement of photothermal conversion efficiency

The setup to measure the photothermal conversion efficiency is depicted in Scheme 1. A quartz cuvette (1 cm × 1 cm × 4 cm), which offered a 10 mm light path, was filled with the nanoparticle solution, with a magnetic stir bar inside. In order to reduce heat loss, the cuvette was covered with foam plastic, with a pinhole to allow the laser light to pass through. A continuous semiconductor diode laser (785 nm, FC-785-500, SFOLT Co. Ltd, China) was coupled to an optical fibre with a light spot of diameter 7.5 mm. The nanoparticle solution was illuminated by the laser, and a power meter was used to measure the laser power. A K-type thermocouple probe (TP02A) was connected to a digital thermometer (TM902C) to record the temperature of the nanoparticle solution as a function of time. The probe head was completely immersed in the solution, but away from the laser illumination area. During the measurement, a small, Teflon-coated magnetic bar was kept stirring to eliminate water temperature gradients in the sample cell.

2.5 DDA simulations

DDA was used as a theoretical tool for the quantitative study of the optical properties of gold nanostructures of various shapes and sizes. DDA calculations were performed using OpenDDA software, running on a Linux system.[49] The size and shape of the gold nanostructures were assumed to be identical to the TEM images and the gold nanostructures were described by 3D Cartesian coordinates. Typically, GNRs were modelled as cylinders with hemispherical caps, lying along the *x*-axis. GNSs were modelled as spheres with six symmetrical branches fixed along the x_+, x_-, y_+, y_-, z_+ and z_- directions, respectively, and with paraboloid section planes. The gold nanostructures were divided into meshes of about 1 nm in size, and the incident light was polarized along the *x* axis. The gold dielectric parameters were fitted using an interpolation method based on experimental dielectric data tabulated by Palik.[50] As the solvent was water, the refractive index of the surrounding medium was 1.333. The optical properties of GNRs and GNSs were quantified in terms of extinction efficiency and absorption efficiency in the wavelength range of 400 to 1100 nm, the same range as for UV-visible extinction spectroscopy.

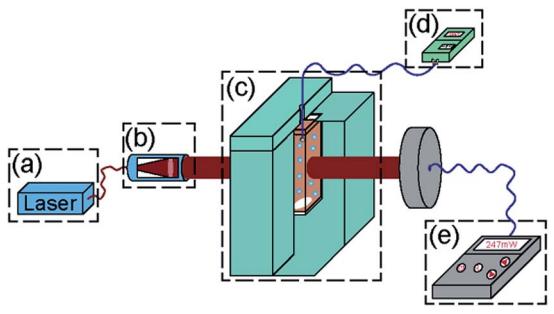

Scheme 1 Apparatus for measurement of the photothermal conversion efficiency of gold nanostructures. (a) Semiconductor diode laser with optical fibre outputting light with a central wavelength of 785 nm. (b) Lenses implanted in a hollow cylinder to change the light to a parallel beam. (c) Sample cell, a quartz cuvette coated with foam plastic. (d) A thermometer with a K-type thermocouple probe to measure the temperature of the sample solution. (e) A power meter to record the laser power before and after the sample solution.

3. Results and discussion

We prepared three GNS samples and three GNR samples, and these six gold nanostructures were classified into three groups according to their central extinction wavelength (S-Group, M-Group, and L-Group). Each group included a GNS and a GNR sample exhibiting similar longitudinal plasmon wavelengths (Fig. 1a). In general, GNR samples have a relatively narrower peak width than GNS samples, corresponding to the better monodispersity of GNRs. Fig. 1b shows TEM images of the GNS and GNR samples. To estimate the volumes of the GNRs, the morphology of more than 100 nanorods was surveyed. Because of the irregular growth of GNSs, it is difficult to measure volume from TEM images. It was therefore assumed that each GNS grows from a single seed, and the GNS volume was obtained from the total amount of gold in the growth solution. Table 1 presents the longitudinal plasmon peak position, concentration and average volume of each gold nanostructure sample. S-GNS shows fewer tips and is smaller in volume compared to M-GNS and L-GNS. The tip number of each GNS is not constant, and the distribution of the shape and position of the tips varies. When the volume of GNS is small, the core makes a significant contribution to the extinction spectroscopy, and the extinction spectrum shows two marked peaks. As the volume of GNS increases, the number of tips increases and the effect of the core on the extinction spectrum gradually decreases. Hence, the extinction peaks of M-GNS and L-GNS are generally much wider than those of S-GNS, the first extinction peak disappears, and a general extinction appears across the whole spectral range. For GNRs, the average aspect ratios for S-GNR, M-GNR and L-GNR are 2.65, 3.78 and 4.18, respectively. With increasing aspect ratio, the volumes of these three GNR samples decreased. By changing the concentrations of the GNS and GNR solutions, the extinction intensities of the longitudinal plasmon peaks were adjusted to be between 0.8 and 1.0, which guaranteed that reasonable laser power could be recorded behind the quartz cuvette in the photothermal measurements. The concentrations of these GNS and GNR samples varied from ~10 pM to ~500 pM, as displayed in Table 1.

To calculate photothermal conversion efficiency, we used a macroscopic model similar to the ones described previously.[51–54] At any moment, the energy balance equations are described as follows:

$$E_{ext} = E_{abs} + E_{sca} \quad (1)$$

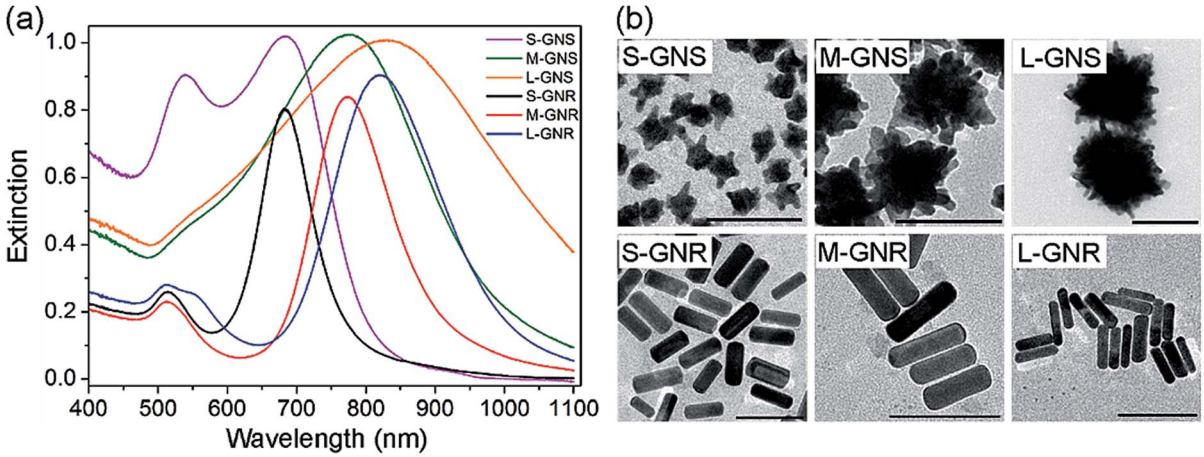

Fig. 1 (a) UV-visible extinction spectra (cell path length: 1.0 cm) of the three groups of GNS and GNR samples. In each group, GNS and GNR showed similar longitudinal plasmon peaks. (b) TEM images of typical GNS and GNR samples used for photothermal conversion efficiency measurements. The scale bar of all the images is 100 nm. The average lengths/diameters of the GNRs are 63.8 nm/24.5 nm, 70.1 nm/19.0 nm, and 56.9 nm/13.9 nm, respectively.

Table 1 Morphological characteristics of gold nanostructures with representative longitudinal plasmon resonance peaks, the laser power after passing through the sample cell and the extinction at 785 nm by the GNSs and GNRs. In this table, c represents the concentration of sample solution, and V represents the average volume of a single gold nanoparticle

GNS/GNR	Peak [nm]	c [pM]	V [nm^3]	Laser power [mW]	Extinction
S-GNS	684.0	504.91	9483.5	126	0.2923
M-GNS	774.5	29.15	115 268	22	1.0503
L-GNS	829.0	10.73	455 290	23	1.0310
S-GNR	683.0	59.07	32 159	151	0.2137
M-GNR	774.0	87.63	20 557	48	0.7115
L-GNR	821.0	176.10	8993.5	54	0.6603

$$E_{abs} = \sum_i m_i C_{p,i} \frac{dT}{dt} + E_{loss} \quad (2)$$

where E_{ext}, E_{abs} and E_{sca} are the extinction, absorption and scattering energies of the nanostructures, respectively, and m_i and $C_{p,i}$ are the mass and heat capacity of each composition of the sample cell, using the constant pressure heat capacity of water for the nanostructure solution. The solution parameters were $m_s = 3.7$ g and $C_{p,s} = 4.187\ J \times g^{-1} \times K^{-1}$, and, for the quartz cuvette, $m_q = 6.4292$ g and $C_{p,q} = 0.839\ J \times g^{-1} \times K^{-1}$. T is the temperature, t is the time, and E_{loss} is the energy dissipated to the atmosphere. E_{ext}, E_{abs} and E_{loss} can be expressed as follows:

$$E_{ext} = P(1 - 10^{-E}),\ E_{abs} = \eta E_{ext},\ E_{loss} = hS_A(T - T_0)$$

where P is the incident infrared laser power, E is the extinction by the nanostructure solution, η is the photothermal conversion efficiency, h is the heat transfer coefficient, S_A is the cross-sectional area perpendicular to the laser illumination, and T_0 is the ambient temperature. Then eqn (2) can be recast as follows:

$$P(1 - 10^{-E})\eta = \sum_i m_i C_{p,i} \frac{dT}{dt} + hS_A(T - T_0) \quad (3)$$

Defining T^* as the temperature difference $(T\text{–}T_0)$, eqn (3) takes a simpler form:

$$\frac{dT^*}{dt} = a - bT^* \quad (4)$$

In this equation, a is the rate of absorption energy and b is the rate constant related to heat loss:

$$a = \frac{P(1 - 10^{-E})\eta}{\sum_i m_i C_{p,i}},\quad b = \frac{hS_A}{\sum_i m_i C_{p,i}} \quad (5)$$

Integrating eqn (4) from 0 to t results in eqn (6), which expresses the curve of temperature change in exponential form:

$$T(t) = T_0 + \frac{a}{b}[1 - \exp(-bt)] \quad (6)$$

Fitting the temperature curve to the data, the values of a and b can be obtained and used to calculate the experimental photothermal conversion efficiency η:

$$\eta = \frac{a \sum_i m_i C_{p,i}}{P(1 - 10^{-E})} \quad (7)$$

It is notable that, because the whole mass of the quartz cuvette does not contribute to the rise in temperature, a calibration of its effective mass needs to be done. In the calibration experiment, the laser was replaced with a resistance, which was connected to a battery and immersed in the solution. It is assumed that the resistance R converts electrical energy into heat completely, *i.e.* E and the conversion efficiency η tend to be

infinite and 1, respectively. Here, it is worth noting that the battery should have small internal resistance, ensuring that the resistance has the dominant differential voltage U. Then the parameter a can be expressed simply as:

$$a = \frac{P}{\sum_i m_i C_{p,i}} \quad (8)$$

In eqn (8), the power P is taken to be the heat power of the resistance, which is proportional to U^2 and inversely proportional to R.

In the calibration experiment, the resistance of 30.31 Ω had a differential voltage of 3.577 V. Therefore, the heat power of the resistance was 422 mW. The temperature was recorded every 30 s for 10 min as soon as the circuit was in operation, and the data is shown in Fig. 2a. By fitting the temperature change curve to an exponential function, the parameter a in eqn (8) is found to be 0.02562. Therefore the effective mass of the quartz cuvette can be calculated, and is $m_{q\text{-eff}} = 1.1741$ g, less than 1/5 of the real mass of the cuvette.

To check the relationship between the parameter a and the heating power P, several other resistances were used to create different heating powers. The relationship is illustrated in Fig. 2b, and shows that a is power-dependent. The ratio of the heating power to a is constant, which means that the effective mass of the quartz cuvette is constant.

With the calibration measurement, representative curves of the temperature change of the GNS and GNR solutions in the photothermal experiments can be obtained, and these are displayed in Fig. 3a. In addition, the temperature change of water under laser illumination was measured. The temperature of the samples was recorded at different times, and all starting points were set as $t = 0$. As the temperature of the environment was different for each sample, the starting temperature was different for each curve. The power of the laser light was measured before and after passing through the sample cell to calculate the extinction intensity E of the GNSs and GNRs according to the logarithm of the ratio of the laser power, *i.e.* $E = \log_{10}(I_w/I_s)$, where I_w and I_s are the laser power after water and after the sample solution, respectively.

The laser power before reaching the sample cell is 270 mW. The laser power I_w after the sample cell containing water is 247 mW. Table 1 lists the laser power after the sample cell and the extinction by the six gold nanostructures as obtained in the photothermal measurements. Temperature variations for the three groups of samples are shown in Fig. 3b. As the extinction peaks for S-GNS and S-GNR are away from 785 nm, their extinction values at 785 nm are much smaller than 1, which

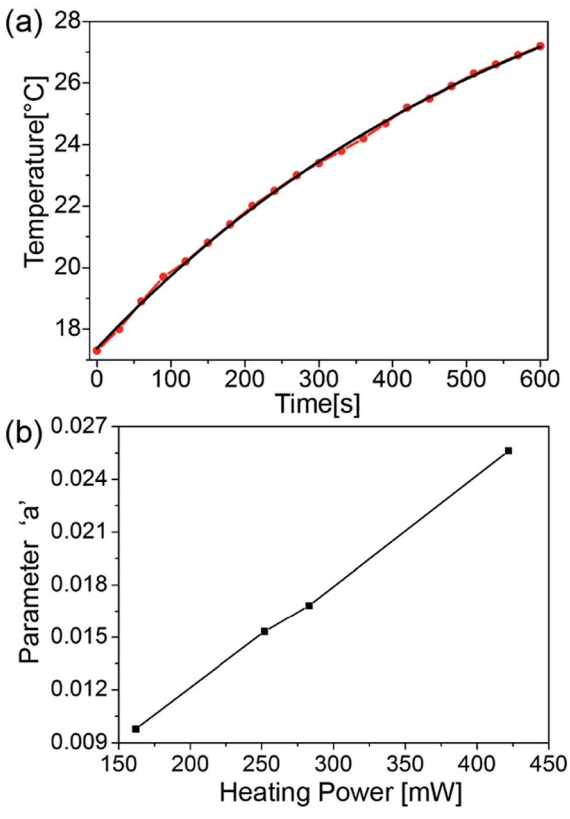

Fig. 2 (a) The temperature change of water (red line and dots) as a function of time, and exponential fitting (black line) used to calibrate the effective mass of the quartz cuvette without laser illumination for the photothermal measurements of GNSs and GNRs. (b) The relationship between the parameter a and the heating power P.

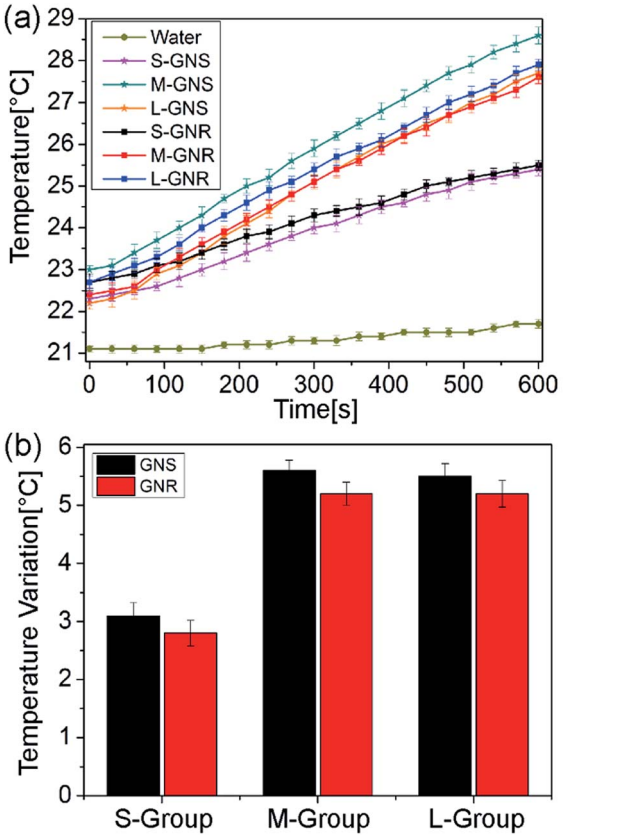

Fig. 3 (a) Experimental data for GNSs and GNRs in aqueous solution under laser illumination, for calculation of the photothermal conversion efficiency. (b) Temperature variation comparison for GNSs (black bars) and GNRs (red bars) in three groups.

results in a lower temperature variation than for the M-group and L-group. Using the concentrations in Table 1 and the temperature variations in Fig. 3b, the molar heating rate can be calculated as the temperature variation divided by the concentration (Fig. 4). With the lowest concentration among all the six samples, L-GNS has the largest molar heating rate, more than 17 times larger than that of L-GNR. The difference between the molar heating rates indicates that the temperature in a localized environment containing a specific concentration of L-GNS will rise much faster than with the same concentration of L-GNR. As to S-GNS, its molar heating rate is smallest. In the M-group, the molar heating rate of GNS is about 3 times larger than that of GNR. In general, GNSs with large volume have a notable advantage in molar heating rate over GNRs with the same longitudinal plasmon peaks.

By fitting the temperature change curves of GNSs and GNRs, the parameter a in eqn (5) can be obtained for each sample, and the photothermal conversion efficiency can be calculated according to eqn (7); this is shown in Fig. 5a. Whether for GNSs or GNRs, the photothermal conversion efficiency decreases as the extinction peaks move from the visible region to the NIR region. The photothermal conversion efficiency of the S-group is higher than that of the M-group and L-group. In the S-group, S-GNR has a photothermal conversion efficiency of 94.2%, which is the highest among all six gold nanostructures. Although the photothermal conversion efficiency of S-GNS is lower than that of S-GNR, it is higher than that of the M-group and L-group. As to the M-group, the photothermal conversion efficiency of both GNS and GNR is over 70%. The L-group has a photothermal conversion efficiency over 65%, which is about 1/3 lower than that of S-GNR. Considering the effect of particle volume on photothermal conversion efficiency, the results are similar for these three groups. For each group, the photothermal conversion efficiency of GNS is lower than that of GNR, while the average volume of GNS is bigger than that of GNR, and this is coincident with previous research.[25,51] The difference in photothermal conversion efficiency between GNS and GNR varies for the three groups. Only in the S-group does the photothermal conversion efficiency show a big gap between GNS and GNR. As the extinction peaks move to the NIR region, the efficiency gap between GNS and GNR becomes narrower, at 5.5% and 4.5% for the M-group and L-group, respectively.

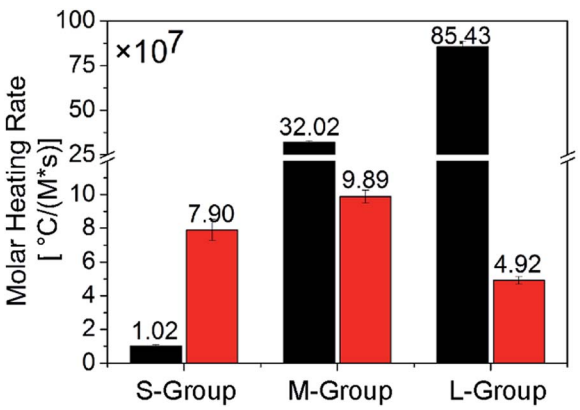

Fig. 4 The molar heating rate of the GNSs (black bar) and GNRs (red bar) as the result of the temperature variation divided by the concentration.

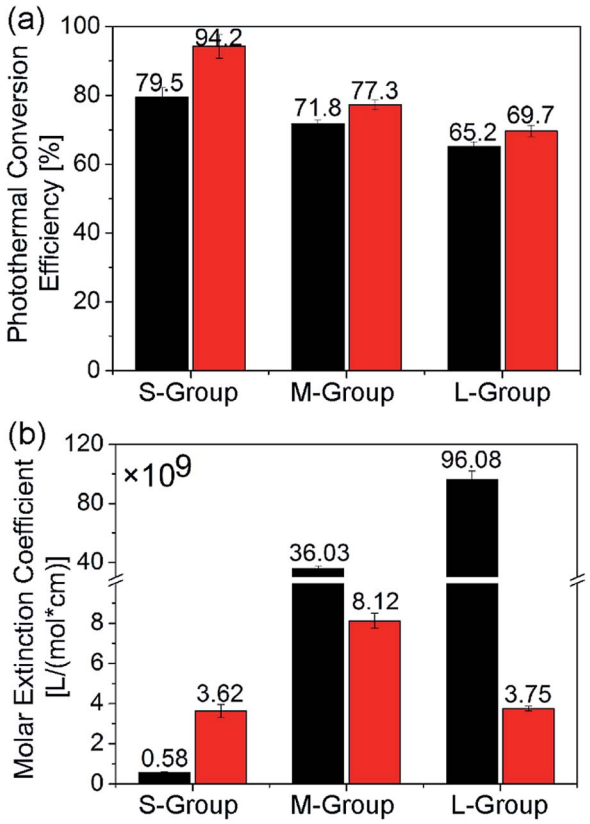

Fig. 5 (a) Photothermal conversion efficiency of GNSs (black bars) and GNRs (red bars), calculated using eqn (7) from exponential fitting results. (b) The molar extinction coefficient of GNSs (black bars) and GNRs (red bars), calculated from the Lambert–Beer law.

According to the Lambert–Beer law, the extinction intensity of a sample solution can be described by eqn (9):

$$E = \varepsilon_{ext} c l \quad (9)$$

In eqn (9), ε_{ext} is the molar extinction coefficient of the gold nanoparticles, c is the molar concentration of the gold nanostructure solution, and l is the light path length. The molar concentration and the extinction intensity of the gold nanoparticles are shown in Table 1. The optical path in our experiment is 10 mm. From the experimental data, the molar extinction coefficients of GNSs and GNRs can be calculated, and the comparison is displayed in Fig. 5b. In the S-group, whose plasmon peaks are away from 785 nm, the molar extinction coefficient of S-GNR is larger than that of S-GNS, while, for both the M-group and the L-group, GNSs have greater molar extinction coefficients than GNRs. For the M-group, the molar extinction coefficient of M-GNS is about 4.5 times larger than that of M-GNR. And in the L-group, the gap between the molar extinction coefficient of L-GNS and L-GNR broadens, *i.e.* L-GNS has a more noticeable advantage over L-GNR. One main factor

in the large molar extinction coefficients of M-GNS and L-GNS is that they occupy large volumes (Table 1). What's more, because of their attractive molar extinction coefficients and modest photothermal conversion efficiencies, M-GNS and L-GNS have a promising advantage in transducing electromagnetic energy to heat, which indicates that they are prospective candidates in the field of photothermal therapy.

It is notable that the molar heating rate has a close relation with the molar extinction coefficient and the photothermal conversion efficiency. L-GNS, for example, has the largest molar extinction coefficient, which means that it has a strong ability to capture electromagnetic energy. At the same time, it has a modest photothermal conversion efficiency, so it is able to convert electromagnetic energy into heat effectively. Therefore, the molar heating rate is a more practical parameter, compared to the photothermal conversion efficiency, to evaluate the photothermal properties of different nanostructures in the biomedical realm.

It is generally known that the Avogadro constant N_A connects the macroscopic quantity and the microscopic quantity. The molar extinction coefficient ε_{ext} is a statistical optical parameter of gold nanoparticles, corresponding to the single nanoparticle extinction coefficient ε_{ext_s}, defined as ε_{ext}/N_A. It is notable that the single nanoparticle extinction coefficient has the same dimensions as absorption cross section. Considering the logarithm bases of the experimental and theoretical extinction

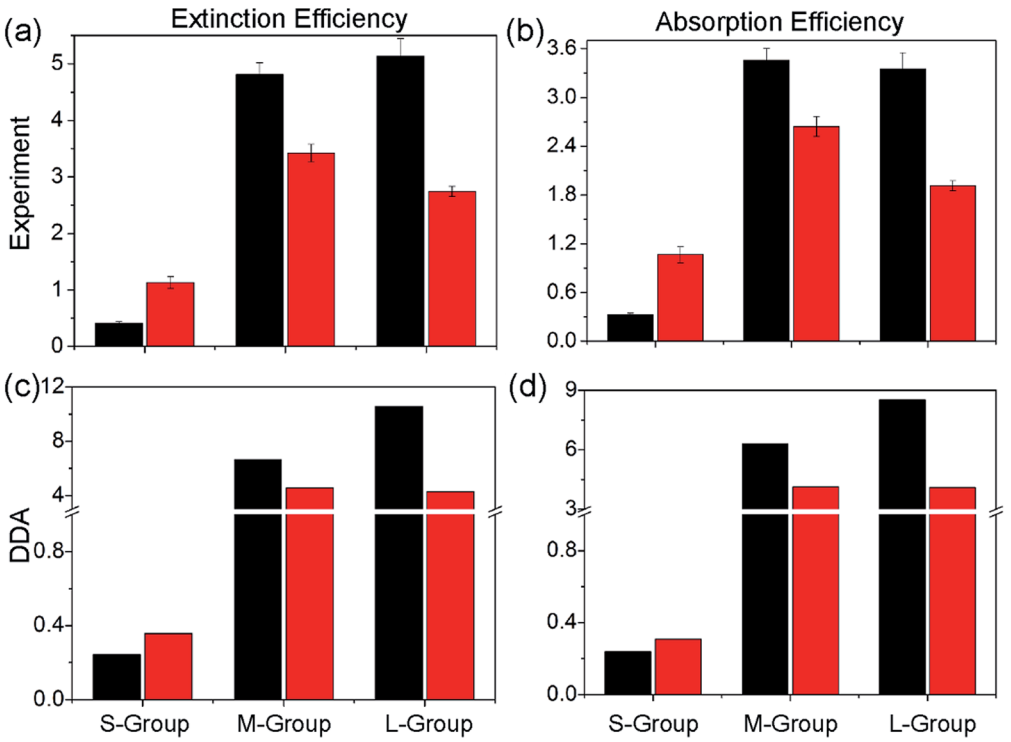

Fig. 6 The typical optical parameters of GNSs (black bar) and GNRs (red bar), including extinction efficiency and absorption efficiency, calculated both from experimental measurements (a, b) and DDA simulations (c, d), respectively.

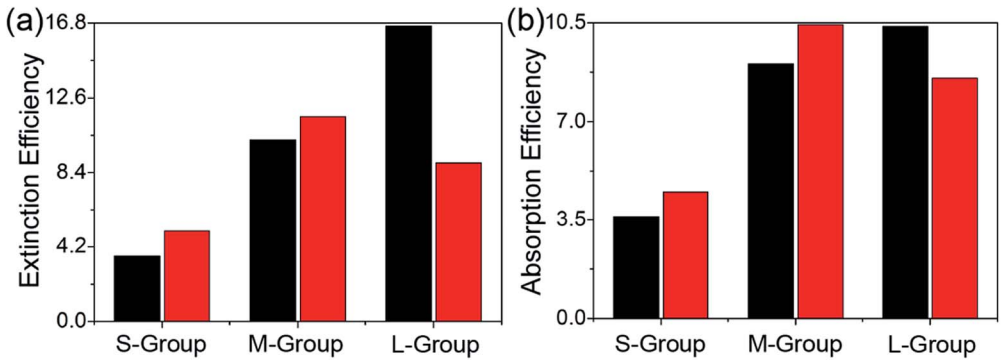

Fig. 7 Simulated extinction efficiencies (a) and absorption efficiencies (b) of GNSs (black bars) and GNRs (red bars) at their respective central plasmon resonant peaks.

coefficients, the experimental extinction cross section may be written as $C_{ext} = \tau\varepsilon_{ext\_s}$, where τ is a constant, equal to ln 10. Furthermore, extinction efficiency can be defined as the extinction cross section divided by the effective cross-sectional area, *i.e.* $Q_{ext} = C_{ext}/\Pi_{eff}$. As noted elsewhere,[25] photothermal conversion efficiency represents the effect of absorption in the extinction, so absorption efficiency can be given as $Q_{abs} = \eta Q_{ext}$ with the help of the photothermal conversion efficiency. Hence, a set of experimental optical parameters for gold nanoparticles can be obtained. At the same time, DDA is a practical tool to simulate the optical properties of gold nanoparticles, and it outputs the extinction and absorption efficiencies of samples. Therefore, DDA calculations were carried out to compare the theoretical optical parameters with the experimental ones.

The comparison of optical parameters of GNSs and GNRs is displayed in Fig. 6, in which the first two frames are calculated from the photothermal measurement data and the others are simulated using DDA. In Fig. 6a and b, M-GNS and L-GNS hold a slender advantage over M-GNR and L-GNR, which means that M-GNS and L-GNS have promising prospects in the field of photothermal therapy. In Fig. 6a, the extinction efficiency of S-GNS is lower than that of S-GNR, while the extinction efficiency of M-GNS is larger than that of M-GNR and the difference broadens in the L-group. The same trend is displayed again for absorption efficiency in Fig. 6b. In all three groups, M-GNS and L-GNS possess higher absorption efficiencies than M-GNR and L-GNR. The difference between theoretical and experimental results may seem surprising at first glance. However, it should be noted that DDA simulates the optical properties of a single nanoparticle, whereas the photothermal measurement is of a statistical phenomenon. Furthermore, there are discrepancies between the real morphology of gold nanostructures and the geometric models applied in the DDA simulations. In Fig. 6c and d, although the parameters of S-GNS have no obvious superiority when compared with S-GNR, yet M-GNS and L-GNS have similar optical properties to M-GNR and L-GNR, which indicates that M-GNS and L-GNS can be used as photothermal agents like GNRs. As the central extinction peak of the S-group is away from the laser wavelength, the extinction efficiencies of S-GNS and S-GNR are small at 785 nm, and their application for photothermal therapy is limited, despite their high photothermal conversion efficiency. According to both experimental and theoretical results, M-GNS and L-GNS show higher extinction efficiencies and absorption efficiencies than M-GNR and L-GNR, indicating that M-GNS and L-GNS are promising materials for the photothermal treatment of cancer and tumours.

From the comparative study of GNSs and GNRs, the S-group generally has few advantages, except for photothermal conversion efficiency, and this is because the central plasmon resonant peak of the S-group is far away from the NIR laser wavelength. To check the photothermal properties at the plasmon peak, DDA was used to calculate the extinction efficiencies and the absorption efficiencies of all three groups of gold nanostructures at their own central plasmon resonant peaks, and the simulation result is illustrated in Fig. 7. In general, the simulation results are all higher at the plasmon peak than at the NIR laser wavelength. It is obvious that the extinction efficiency and absorption efficiency of the S-group are much larger than those in Fig. 6c and d, while the M-group and L-group do not show large differences between the simulation results at the plasmon peak and at the NIR laser wavelength. The simulation results indicate that the gold nanostructures show the best photothermal performance at their own plasmon resonant peaks. However, as mentioned above, biological tissues are highly transparent to NIR light, while the central plasmon resonant peak of the S-group is in the visible region. Therefore, the optical parameters of the S-group at the central peak are of less practical significance for photothermal therapy.

4. Conclusions

In summary, the temperature variation of three groups of GNSs and GNRs has been recorded with calibration of the effective mass of the container, and the photothermal conversion efficiency of each sample has been calculated according to an exponential model of temperature change. Due to different extinction intensities at the illumination laser wavelength, the aqueous solutions of M-group and L-group gold nanostructures can reach higher temperatures than those of the S-group. The photothermal conversion efficiency of gold nanostructures depends strongly on the morphology, the plasmon resonance wavelength and the nanostructure volume. Although gold nanoparticles in the S-group show higher photothermal conversion efficiencies, gold nanoparticles in the M-group and L-group possess faster molar heating rates and larger molar extinction coefficients, which means that they can satisfy specific heating requirements with less time and fewer nanoparticles. DDA was employed to simulate the optical properties of gold nanoparticles. It should be noted that biological tissues are a highly scattering medium, and our research was conducted in aqueous solution. Nevertheless, both experimental and theoretical results show that GNSs have similar photothermal properties to GNRs, especially for M-GNS and L-GNS, which paves the way for the potential application of GNSs in the field of photothermal cancer therapy.

Acknowledgements

The work was supported by the National Nature Science Foundation of China (grant no. 212731126) and the Fundamental Research Program of Shenzhen (JC201105201112A, JCYJ20120619151629728). Part of this work was supported by the Open Research Fund Program of the State Key Laboratory of Low-Dimensional Quantum Physics (KF201311).

Notes and references

1 T. Seki, M. Wakabayashi, T. Nakagawa, M. Imamura, T. Tamai, A. Nishimura, N. Yamashiki, A. Okamura and K. Inoue, *Cancer*, 1999, **85**, 1694.
2 G. S. Gazelle, S. N. Goldberg, L. Solbiati and T. Livraghi, *Radiology*, 2000, **217**, 633.
3 F. A. Jolesz and K. Hynynen, *Cancer J.*, 2001, **8**, S100.

4 S. M. Waldow, P. R. Morrison and L. I. Grossweiner, *Lasers Surg. Med.*, 1988, **8**, 510.
5 W. R. Chen, R. L. Adams, R. Carubelli and R. E. Nordquist, *Cancer Lett.*, 1997, **115**, 25.
6 R. Puls, C. Stroszczynski, G. Gaffke, N. Hosten, R. Felix and U. Speck, *J. Magn. Reson. Imaging*, 2003, **17**, 663.
7 A. Vogel and V. Venugopalan, *Chem. Rev.*, 2003, **103**, 577.
8 D. P. O'Neal, L. R. Hirsch, N. J. Halas, J. D. Payne and J. L. West, *Cancer Lett.*, 2004, **209**, 171.
9 N. W. S. Kam, M. O'Connell, J. A. Wisdom and H. Dai, *Proc. Natl. Acad. Sci. U. S. A.*, 2005, **102**, 11600.
10 Q. Tian, M. Tang, Y. Sun, R. Zou, Z. Chen, M. Zhu, S. Yang, J. Wang, J. Wang and J. Hu, *Adv. Mater.*, 2011, **23**, 3542.
11 Y. Shen, A. G. Skirtach, T. Seki, S. Yagai, H. Li, H. Möhwald and T. Nakanishi, *J. Am. Chem. Soc.*, 2010, **132**, 8566.
12 L. F. Neves, J. J. Krais, B. D. Van Rite, R. Ramesh, D. E. Resasco and R. G. Harrison, *Nanotechnology*, 2013, **24**, 375104.
13 Z. Sheng, L. Song, J. Zheng, D. Hu, M. He, M. Zheng, G. Gao, P. Gong, P. Zhang and Y. Ma, *Biomaterials*, 2013, **34**, 5236.
14 X.-D. Zhang, D. Wu, X. Shen, J. Chen, Y.-M. Sun, P.-X. Liu and X.-J. Liang, *Biomaterials*, 2012, **33**, 6408.
15 J. Chen, D. Wang, J. Xi, L. Au, A. Siekkinen, A. Warsen, Z.-Y. Li, H. Zhang, Y. Xia and X. Li, *Nano Lett.*, 2007, **7**, 1318.
16 S. E. Skrabalak, J. Chen, Y. Sun, X. Lu, L. Au, C. M. Cobley and Y. Xia, *Acc. Chem. Res.*, 2008, **41**, 1587.
17 M. P. Melancon, W. Lu, Z. Yang, R. Zhang, Z. Cheng, A. M. Elliot, J. Stafford, T. Olson, J. Z. Zhang and C. Li, *Mol. Cancer Ther.*, 2008, **7**, 1730.
18 C. Loo, A. Lowery, N. Halas, J. West and R. Drezek, *Nano Lett.*, 2005, **5**, 709.
19 W. Hasan, C. L. Stender, M. H. Lee, C. L. Nehl and J. Lee, *Nano Lett.*, 2009, **9**, 1555.
20 X. Huang, I. H. El-Sayed, W. Qian and M. A. El-Sayed, *J. Am. Chem. Soc.*, 2006, **128**, 2115.
21 A. M. Alkilany, L. B. Thompson, S. P. Boulos, P. N. Sisco and C. J. Murphy, *Adv. Drug Delivery Rev.*, 2012, **64**, 190.
22 H. Yuan, C. G. Khoury, C. M. Wilson, G. A. Grant, A. J. Bennett and T. Vo-Dinh, *Nanomedicine: Nanotechnology, Biology and Medicine*, 2012, **8**, 1355.
23 F. Zhou, S. Wu, B. Wu, W. R. Chen and D. Xing, *Small*, 2011, **7**, 2727.
24 E. Miyako, K. Kono, E. Yuba, C. Hosokawa, H. Nagai and Y. Hagihara, *Nat. Commun.*, 2012, **3**, 1226.
25 H. Chen, L. Shao, T. Ming, Z. Sun, C. Zhao, B. Yang and J. Wang, *Small*, 2010, **6**, 2272.
26 W. Tao, H. Bao and M. Gu, *Appl. Phys. B*, 2013, **112**, 153.
27 J. Song, L. Pu, J. Zhou, B. Duan and H. Duan, *ACS Nano*, 2013, **7**, 9947.
28 R. S. Norman, J. W. Stone, A. Gole, C. J. Murphy and T. L. Sabo-Attwood, *Nano Lett.*, 2008, **8**, 302.
29 Y. Qiu, Y. Liu, L. Wang, L. Xu, R. Bai, Y. Ji, X. Wu, Y. Zhao, Y. Li and C. Chen, *Biomaterials*, 2010, **31**, 7606.
30 S. Jin, X. Ma, H. Ma, K. Zheng, J. Liu, S. Hou, J. Meng, P. C. Wang, X. Wu and X.-J. Liang, *Nanoscale*, 2013, **5**, 143.
31 J.-Y. Kim, W. I. Choi, M. Kim and G. Tae, *J. Controlled Release*, 2013, **171**, 113.
32 J. Lin, S. Wang, P. Huang, Z. Wang, S. Chen, G. Niu, W. Li, J. He, D. Cui and G. Lu, *ACS Nano*, 2013, **7**, 5320.
33 S. Abalde-Cela, P. Aldeanueva-Potel, C. Mateo-Mateo, L. Rodríguez-Lorenzo, R. A. Alvarez-Puebla and L. M. Liz-Marzán, *J. R. Soc., Interface*, 2010, **7**, S435.
34 C. G. Khoury and T. Vo-Dinh, *J. Phys. Chem. C*, 2008, **112**, 18849.
35 H. Yuan, A. M. Fales, C. G. Khoury, J. Liu and T. Vo-Dinh, *J. Raman Spectrosc.*, 2013, **44**, 234.
36 S. Barbosa, A. Agrawal, L. Rodríguez-Lorenzo, I. Pastoriza-Santos, R. A. Alvarez-Puebla, A. Kornowski, H. Weller and L. M. Liz-Marzán, *Langmuir*, 2010, **26**, 14943.
37 B. Van de Broek, N. Devoogdt, A. D'Hollander, H.-L. Gijs, K. Jans, L. Lagae, S. Muyldermans, G. Maes and G. Borghs, *ACS Nano*, 2011, **5**, 4319.
38 A. M. Fales, H. Yuan and T. Vo-Dinh, *Langmuir*, 2011, **27**, 12186.
39 C. Kim, H.-M. Song, X. Cai, J. Yao, A. Wei and L. V. Wang, *J. Mater. Chem.*, 2011, **21**, 2841.
40 F. Hao, C. L. Nehl, J. H. Hafner and P. Nordlander, *Nano Lett.*, 2007, **7**, 729.
41 R. Rodríguez-Oliveros and J. A. Sánchez-Gil, *Opt. Express*, 2012, **20**, 621.
42 H. Yuan, A. M. Fales and T. Vo-Dinh, *J. Am. Chem. Soc.*, 2012, **134**, 11358.
43 S. Wang, P. Huang, L. Nie, R. Xing, D. Liu, Z. Wang, J. Lin, S. Chen, G. Niu and G. Lu, *Adv. Mater.*, 2013, **25**, 3055.
44 J. Li, J. Han, T. Xu, C. Guo, X. Bu, H. Zhang, L. Wang, H. Sun and B. Yang, *Langmuir*, 2013, **29**, 7102.
45 D. C. Hone, A. H. Haines and D. A. Russell, *Langmuir*, 2003, **19**, 7141.
46 B. Nikoobakht and M. A. El-Sayed, *Chem. Mater.*, 2003, **15**, 1957.
47 T. K. Sau and C. J. Murphy, *Langmuir*, 2004, **20**, 6414.
48 J. Cheng, L. Ge, B. Xiong and Y. He, *J. Chin. Chem. Soc.*, 2011, **58**, 822.
49 J. Mc Donald, A. Golden and S. G. Jennings, *Int. J. High Perform. Comput. Appl.*, 2009, **23**, 42.
50 E. D. Palik, *Handbook of Optical Constants of Solids*, Academic Press, New York, 1985.
51 J. R. Cole, N. A. Mirin, M. W. Knight, G. P. Goodrich and N. J. Halas, *J. Phys. Chem. C*, 2009, **113**, 12090.
52 H. H. Richardson, M. T. Carlson, P. J. Tandler, P. Hernandez and A. O. Govorov, *Nano Lett.*, 2009, **9**, 1139.
53 D. K. Roper, W. Ahn and M. Hoepfner, *J. Phys. Chem. C*, 2007, **111**, 3636.
54 D. K. Kim, M. S. Amin, S. Elborai, S.-H. Lee, Y. Koseoglu, M. Zahn and M. Muhammed, *J. Appl. Phys.*, 2005, **97**, 10J510.